

See discussions, stats, and author profiles for this publication at: <https://www.researchgate.net/publication/311879245>

Paleofloods records in Himalaya

Article *in* Geomorphology · December 2016

DOI: 10.1016/j.geomorph.2016.12.011

CITATION

1

READS

290

15 authors, including:



[Pradeep Srivastava](#)

Wadia Institute of Himalayan Geology

86 PUBLICATIONS 1,341 CITATIONS

[SEE PROFILE](#)



[Anil Kumar](#)

Wadia Institute of Himalayan Geology

17 PUBLICATIONS 16 CITATIONS

[SEE PROFILE](#)



[Narendra Kumar Meena](#)

Wadia Institute of Himalayan Geology

12 PUBLICATIONS 64 CITATIONS

[SEE PROFILE](#)



[Suman Rawat](#)

Wadia Institute of Himalayan Geology

8 PUBLICATIONS 64 CITATIONS

[SEE PROFILE](#)

Some of the authors of this publication are also working on these related projects:



Attempting to understand paleo-agriculture from archaeological sites using variety of chemical and isotopic tracers to gain insights to complex Human-Culture-Climate relationship [View project](#)



Late Quaternary evolution of the Alaknanda valley in the vicinity of North Almora Thrust, [View project](#)

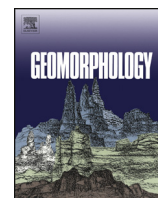
All content following this page was uploaded by [Anil Kumar](#) on 02 March 2017.

The user has requested enhancement of the downloaded file. All in-text references [underlined in blue](#) are added to the original document and are linked to publications on ResearchGate, letting you access and read them immediately.



Contents lists available at ScienceDirect

Geomorphology

journal homepage: www.elsevier.com/locate/geomorph

Paleofloods records in Himalaya

P. Srivastava^{a,*}, A. Kumar^a, S. Chaudhary^b, N. Meena^a, Y.P. Sundriyal^c, S. Rawat^a, N. Rana^c, R.J. Perumal^a, P. Bisht^c, D. Sharma^c, R. Agnihotri^d, D.S. Bagri^c, N. Juyal^e, R.J. Wasson^f, A.D. Ziegler^g

^a Wadia Institute of Himalayan Geology, 33 GMS Road, Dehradun, India

^b Centre for Earth Sciences, Indian Institute of Science, Bangalore 560012, India

^c HNB Garhwal University, Srinagar, Garhwal, India

^d Birbal Sahni Institute of Palaeosciences, Lucknow 226007, India

^e Physical Research Laboratory, Ahmedabad 308009, India

^f Institute of Water Policy, Lee Kuan Yew School of Public Policy, NUS, Singapore

^g Geography Department, National University of Singapore, Singapore

ARTICLE INFO

Article history:

Received 21 March 2016

Received in revised form 1 December 2016

Accepted 14 December 2016

Available online xxx

Keywords:

Paleofloods

Himalayan rivers

Chronology

Paleoclimate

GLOF

LLOF

ISM

ABSTRACT

We use paleoflood deposits to reconstruct a record of past floods for the Alaknanda-Mandakini Rivers (Garhwal Himalaya), the Indus River (Ladakh, NW Himalaya) and the Brahmaputra River (NE Himalaya). The deposits are characterized by sand-silt couplets, massive sand beds, and from debris flow sediment. The chronology of paleoflood deposits, established by Optically Stimulated Luminescence (OSL) and ¹⁴C AMS dating techniques, indicates the following: (i) The Alaknanda-Mandakini Rivers experienced large floods during the wet and warm Medieval Climate Anomaly (MCA); (ii) the Indus River experienced at least 14 large floods during the Holocene climatic optimum, when flood discharges were likely an order of magnitude higher than those of modern floods; and (iii) the Brahmaputra River experienced a megaflood between 8 and 6 ka. Magnetic susceptibility of flood sediments indicates that 10 out of 14 floods on the Indus River originated in the catchments draining the Ladakh Batholith, indicating the potential role of glacial lake outbursts (GLOFs) and/or landslide lake outbursts (LLOFs) in compounding flood magnitudes. Pollen recovered from debris flow deposits located in the headwaters of the Mandakini River showed the presence of warmth-loving trees and marshy taxa, thereby corroborating the finding that floods occurred during relatively warm periods. Collectively, our new data indicate that floods in the Himalaya largely occur during warm and wet climatic phases. Further, the evidence supports the notion that the Indian Summer Monsoon front may have penetrated into the Ladakh area during the Holocene climatic optimum.

© 2016 Elsevier B.V. All rights reserved.

1. Introduction

Under the influence of the Indian Summer Monsoon (ISM), rivers originating in the Himalaya and Tibet are susceptible to flooding. Therefore, >15% of the world's population, which is supported by the major Himalayan rivers, including the Indus, Ganga, Brahmaputra and Yangtze, are at risk from flooding (Webster et al., 2011). As an example, in the Garhwal Himalaya extreme rainfall in 2013 led to the most catastrophic flood of the millennium (Sundriyal et al., 2015; Ziegler et al., 2014). In general, large floods in the Upper Ganga Catchment are frequent. For example, there have been two significant 'flash' floods in the recent history of the Alaknanda River (1894 and 1970; Wasson et al., 2008; Rana et al., 2013) prior to the 2013 event. Further, paleoflood deposits show that there have been 12 major floods on the Alaknanda in the last 800 years – equivalent to more than one every century (Wasson

et al., 2008, 2013). The frequency of flooding in the upper Ganga, as well as other large Himalayan rivers, demonstrates the need for long-term records of high-magnitude floods to assess flood risk in the Himalayan region – an area where even short-term discharge and rainfall records are rare (Negi, 2002).

Paleoflood hydrology enables the extension of flood histories beyond the instrumental records and thus can provide long-term records of flood frequency, magnitude and trends (Kochel and Baker, 1982). Floods in the Himalaya often occur in response to heavy rainfall during the annual monsoon period or as a result of a monsoon anomaly (Kale, 2004; Ziegler et al., 2014). According to Rasmussen and Houze (2012), flash floods result from a myriad of storm types with differing structures and synoptic conditions (cf. Doswell, 1985; Doswell et al., 1996; Maddox et al., 1978). For example, the 2010 flash flood event in Ladakh (upper Indus) was caused by a large (meso-scale) rain-producing cloud system that formed over the high Himalaya and Tibetan Plateau, and received additional moisture from monsoon air masses moving northward from the Arabian Sea and Bay of Bengal (Rasmussen and Houze,

* Corresponding author.

E-mail address: pradeep@wihg.res.in (P. Srivastava).

2012). A more recent event in 2015 had a slightly different genesis. A mesoscale convective cell developed over the Tibetan Plateau, and the moist air mass over the plateau prior to cell development originated from westerly upper-air advection of water vapour from previous storms along the Indo-Pakistan border (Ziegler et al., 2016). In the case of the 2013 flood and debris flows in the Mandakani River (upper Ganges), an early monsoon incursion into the high Himalaya combined with a surge of cold Arctic air destabilized the atmosphere and resulted in heavy rainfall in the high mountains (Joseph et al., 2014).

In general, many Himalayan floods are produced by breaches of landslide and glacially dammed lakes (Korup et al., 2006; Gupta and Sah, 2008). Glacial lake outburst floods (GLOFs) are caused by the breaching or overflow of a lake formed due to damming by a glacier or its older moraines. Landslide lake outburst floods (LLOFs) are analogous, with the dams being formed by landslides. The breaching of a moraine-dammed lake compounded the flood magnitude in the upper reaches of the Mandakani River in 2013 (Dobhal et al., 2013; Sundriyal et al., 2015; Sati and Gahalaut, 2013; Joseph et al., 2014).

Sedimentological records of past flood events are preserved as slack water deposits (SWDs; Srivastava et al., 2008; Wasson et al., 2013), massive sand beds on fluvial terraces (Montgomery et al., 2004; Lang and Huntington, 2014), and debris flow deposits, many of which are associated with dam breaching (Bookhagen et al., 2005; Phartiyal et al., 2009; Dortch et al., 2011; Srivastava et al., 2013). The occurrences of landslides and the damming of rivers in the Tethyan Himalaya and

Garhwal Himalaya are reported to have occurred during phases of a strengthened ISM (Sundriyal et al., 2007; Dortch et al., 2009; Phartiyal et al., 2009; Srivastava et al., 2013). Similarly, historical records from the Ladakh Himalaya indicate that 71 GLOF and LLOF events have occurred since 1826 (see Hewitt, 1988, 1998). However, studies of sedimentological records of Holocene floods in the Himalaya are rare though data exists from the Alaknanda and Brahmaputra rivers (Srivastava et al., 2008; Wasson et al., 2013; Lang et al., 2013). The time scale of the Holocene is especially important, as it has witnessed an exponential increase in landscape-human interaction, with both droughts and floods increasingly impacting on settlements and possibly causing migration (Hawks et al., 2007; Johnson and Brook, 2011).

This study presents new evidence of paleofloods and their ages in three rivers of the Himalaya: (i) the Alaknanda and Mandakini Rivers (major tributaries of the Ganga River system); (ii) the Indus River, where for the first time SWDs are reported; and (iii) the Brahmaputra River, where massive sand deposits are indicators of megafloods (Fig. 1a). Further, we examine the total ensemble of present and published records of paleofloods, including historical archives of Hewitt (1988, 1999), in the context of historical variability of the Indian Summer Monsoon. We combine the ages, sedimentological characteristics, and location of several paleoflood deposits with published records of outburst floods to reconstruct the flood history of the region for the past 14,000 years, which extends back before the Holocene. Draining distinctly different regions, the three chosen rivers form a spectrum from

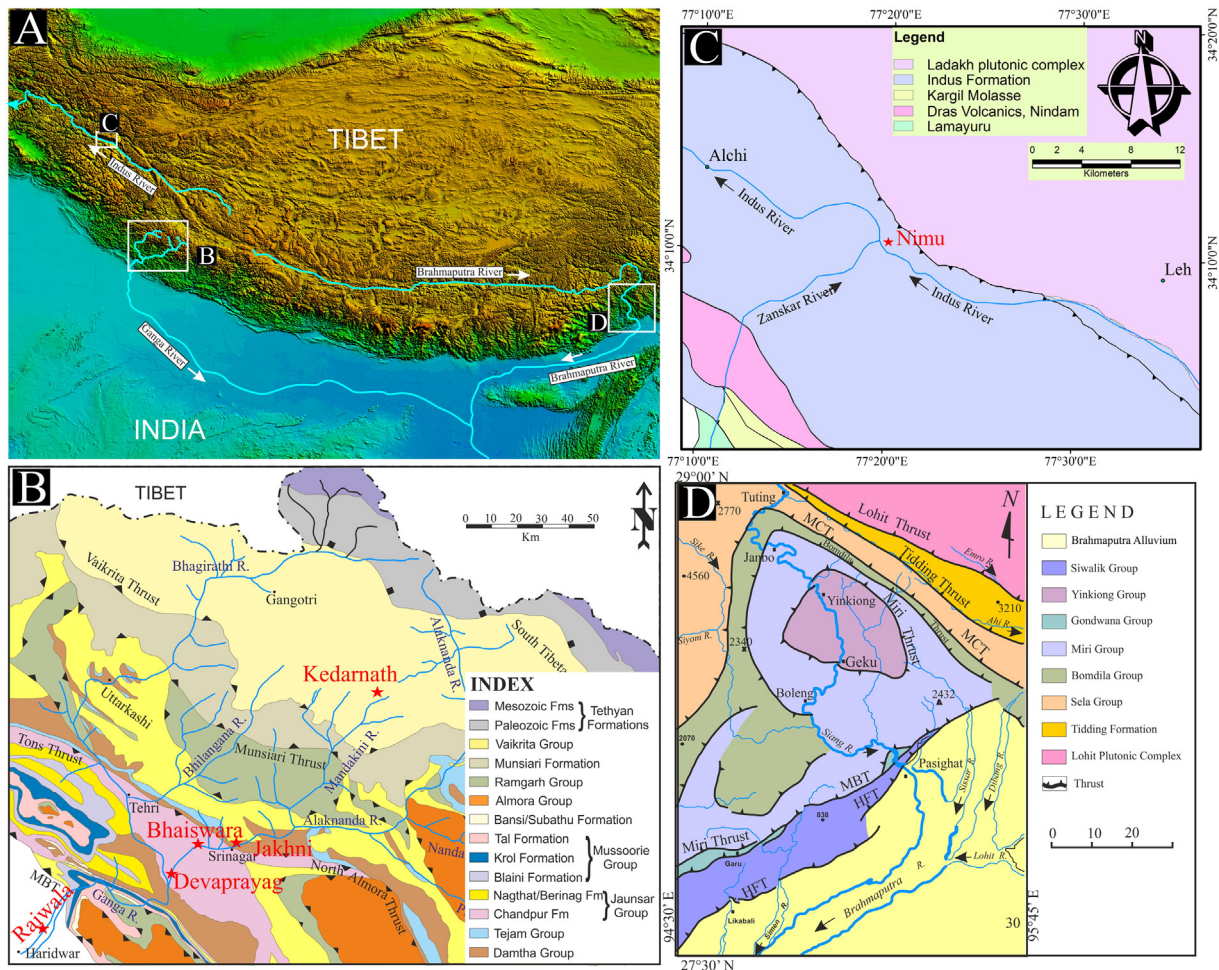


Fig. 1. (A) Satellite image showing the study locations in the Indus, the Alaknanda-Mandakini and the Brahmaputra river systems in the Himalaya. (B) Detailed geological map of Alaknanda-Mandakini river valleys showing locations of paleoflood deposits at Kedarnath, Jakhni, Bhaiswara, Deoprayag and Raiwala. (C) Geological map showing study site of Nimu, Indus river, Ladakh. Note the two lithologies, granitic Batholith in the north and Molasse in the south with Upshi-Basgo thrust separating the two. Shown here are the sites from where the river discharges are reported. (D) Geological map showing study locations, Tuting, Yinkiong, Geku, Pasighat in Brahmaputra valley.

arid (Indus River) to sub-humid and humid climates (the Alaknanda, Mandakini and the Brahmaputra rivers) that aids in understanding floods in different climatic regimes of the Himalaya.

2. Geographic setting

The sites investigated in this study are the Alaknanda-Mandakini River system of the Garhwal Himalaya, the Indus River in Ladakh (NW Himalaya), and the Brahmaputra River in the NE Himalaya (Fig. 1). The Alaknanda-Mandakini River system drains the southern front of the Garhwal Himalaya and traverses four tectonic discontinuities in the N-S direction (Fig. 1): the South Tibetan Detachment System (STDS); the Main Central Thrust (MCT); the Main Boundary Thrust (MBT); and the Himalayan Frontal Thrust (HFT). We investigated two previously unstudied river sections: the first at Kedarnath in the headwaters of the Mandakini tributary; and the second at Jakhni in the Alaknanda Valley (Fig. 1b). Herein, we also discuss the section at Bhainswara, also in the Alaknanda valley (Wasson et al., 2013).

The Indus River flows parallel to the Indus Tsangpo Suture Zone (ITSZ) in Ladakh. It makes a deep gorge in the NW Syntaxis of the Himalaya, then flows through the southern front of the Himalaya to the plains of Pakistan before draining into the Arabian Sea. We studied a section in the Zaskar valley a few kilometres upstream of the confluence of the Indus and Zaskar Rivers (Fig. 1c). This is the section where lake outburst events were described by Hewitt and Liu (2010). The Brahmaputra River, in the NE Himalaya, originates in the ITSZ and traverses the NE Syntaxis, making a deep gorge upstream of the MCT, before passing through the MBT and HFT (Fig. 1d). We studied four sections along this river (Fig. 1d): (i) Tuting; (ii) Inkiyong; (iii) Geku; and (iv) Pasighat.

The range in annual precipitation in the Himalaya from north to south and east to west is between $>3000 \text{ mm y}^{-1}$ and $<500 \text{ mm y}^{-1}$. The Garhwal Himalaya (Alaknanda-Mandakini River system) on the southern front of the mountains receives about 1400 mm y^{-1} (Wasson et al., 2013). The Indus River Catchment at Ladakh lies in the rain shadow zone of the ISM, and therefore receives only about 100 mm y^{-1} . Only in abnormal monsoon years, when the monsoon penetrates deep into the mountains, does Ladakh receive higher rainfall (Bookhagen et al., 2005). In the NE Himalaya, the Brahmaputra Valley receives about 2500 mm y^{-1} of precipitation, mainly during the ISM (Gadgil, 2003).

Analysis of data from 1866 to 2006 for the rainfall shadow zone of Ladakh shows that the summer rainfall is significantly correlated with the ISM through the influence of the El-Nino Southern Oscillation (ENSO; Bhutiyani et al., 2010). Similarly, the NE Himalaya receives rainfall that is largely controlled by the ISM and partly aided by the East Asian Monsoon. Consequently, the ISM is the major control of the floods of the Indus, Ganga, and Brahmaputra Rivers. It has been suggested that the frequency of larger floods in the Himalaya increases during wet climatic conditions (Starkel, 1983) and increases during periods of climatic transitions when runoff varies drastically (Teller, 1995). The role of wet periods in generating floods will be explored below.

The Ladakh-Karakorum rain-shadow limits vegetation and makes the area vulnerable to rainfall-induced, river-damming landslides. In addition, surging glaciers in the region often block rivers, forming lakes. During excessive glacial melting and rainfall events such lakes breach causing landslide lake outburst floods (LLOFs) or glacial lake outbursts floods (GLOFs). The earliest inventory of such events was compiled by Mason (1929). A recent review by Hewitt and Liu (2010) lists 71 events of GLOFs and LLOFs since 1826. The frequency plot, with 5 year bins of all events, indicates clusters around 1830, 1900, 1925 and 1970 (Fig. 2a). The tree ring climate record from the rain shadow of the Himalaya indicates that these events cluster during phases of higher than normal rainfall when discharge is correspondingly high (Fig. 2b).

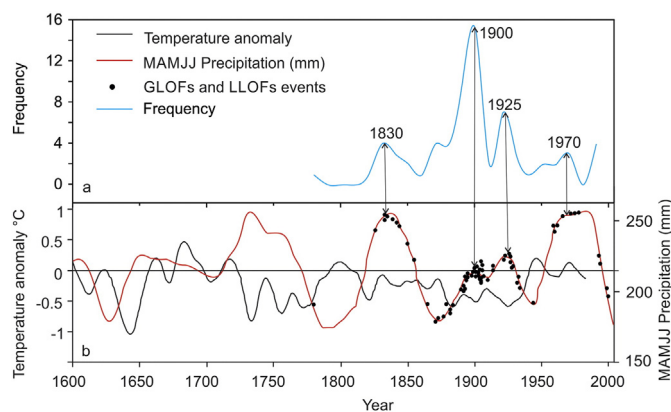


Fig. 2. (a) Historical records of Glacial lake outburst flood (GLOFs) and Landslide lake outburst flood (LLOFs) in Ladakh. (b) Tree ring climate record of rain shadow zone of Himalaya (Singh et al., 2006).

The modern mean discharge of the Indus River for August (2002–2004) at the Leh station ranged from 130 to $250 \text{ m}^3 \text{ s}^{-1}$ with a mean (\pm Stdev) of $198 \pm 45 \text{ m}^3 \text{ s}^{-1}$. Two very large rainfall events (cloud bursts) occurred in August 2006 and August 2010, causing sudden increases in Indus discharge ($1846 \text{ m}^3 \text{ s}^{-1}$ and $1940 \text{ m}^3 \text{ s}^{-1}$, respectively), recorded at Alchi Dam, 20.5 km downstream of Leh (Fig. 3, see Fig. 1c for location). District administration records and published data show that major floods in different catchments of the Indus valley occurred in 1999, 2005, 2006, and 2015 (Juyal, 2010; Hobley et al., 2012; Thayyen et al., 2013). The Indus valley near Leh is one of the widest and most populated segments of the Indus valley in Ladakh.

A large part of the Brahmaputra River catchment lies in Tibet, where its channel is often blocked by moraines of retreating glaciers and massive landslides giving rise to large impoundments with volumes as high as 800 km^3 (Montgomery et al., 2004; Korup and Montgomery, 2008). Breaches of such lakes create megafloods – the large flood in 2000 is a recent example. The flood originated 40 km upstream of the Tsangpo Gorge in the Yigong River. Deposits of the 2000 flood are grey coloured sand and sit on terraces at above-river level (ar1) up to 30 m, situated in the Assam plains along the river (Evans and Delaney, 2011a,b; Lang et al., 2013). Sediments of past megafloods are also seen in sheltered parts of higher terraces (Lang et al., 2013). These sediments occur in 2–8 m thick sequences and consist of parallel laminated or massive yellowish grey medium to fine sand. The tops of the sequences show pedogenic alteration with thick accumulations of organic matter, suggesting that they are the result of older floods. At Tuting, Yingkiang, Geku, Panging, and Pasighat, these deposits are 6–8 m thick (Fig. 1). Petrographic analysis and zircon chronology of these megaflood deposits

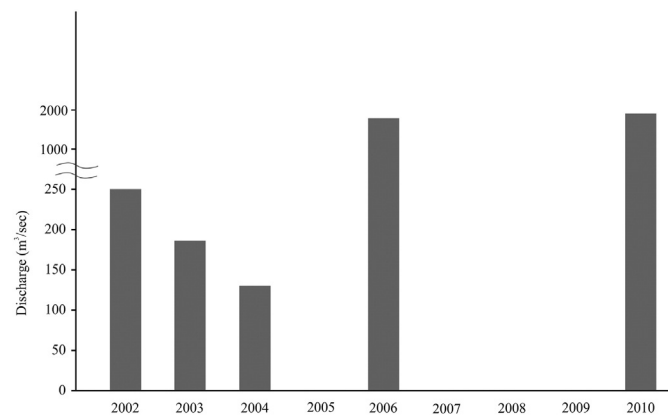


Fig. 3. Discharge data of Indus river.

indicate that they mostly originate in Tibet, and are thus likely linked to GLOFs and LLOFs (Lang et al., 2013).

3. Methods and materials

3.1. Identification of paleoflood deposits

Identification of paleoflood deposits was based on their sedimentological attributes and location. The deposits that were found at the junction of two rivers or in the sheltered zones along channels are Slack Water Deposits (SWDs). Sedimentologically, these deposits are made up of fine-sand and silt or silty clay graded couplets, each one of which represents one flood. Likewise, thick massive sand deposits were found several meters above the river level on top of terrace surfaces at many locations along the Brahmaputra River. We dated these previously reported deposits (Lang et al., 2013) during this study. Colluvial and alluvial fills of such rivers are normally composed of poorly sorted angular gravels and fining-upward imbricated gravels (Ray and Srivastava, 2010), and are hence distinguishable from paleoflood deposits that have distinct sedimentological characteristics. Organic-rich debris flows have poorly sorted, matrix-supported fabrics composed of black organic mud, wood debris, pottery pieces and building materials. These kinds of deposit may show weak bedding structures but do not show bedding or grading.

3.2. Chronology

A combination of Optically Stimulated Luminescence (OSL) and ^{14}C -AMS dating techniques was used to establish the chronology of the paleoflood deposits. OSL dating provides an estimate of the time of burial of sediment (for details see: Aitken, 1998; Srivastava et al., 2008). Briefly, an OSL date requires two types of measurement: (1) luminescence measurements for the estimation of the paleodose (Ed); and (2) a measurement of the annual radiation dose via estimation of dose rate (Aitken, 1998). During sample preparation to separate clean quartz, we utilized a standard chemical pre-treatment, whereby the 90–150 μm fraction of separated quartz was etched using 40% HF for 80 min followed by 12 N HCl treatment for 40 min to remove the alpha affected outer skin of the grains. Feldspar contamination was tested by using Infrared Stimulated Luminescence (IRSL). The samples showing > 100 IRSL counts were subjected to an additional step of etching with 40% HF for 10 min. However, in cases where samples exhibited high IRSL counts an optical cleaning of the feldspar signal was carried out (Ray and Srivastava, 2010).

Luminescence was measured on a Risø TL/OSL-20 system with the blue LEDs emitting at 470 nm. The stimulation was carried out at a sample temperature of 125 °C for 40 s. Light was detected using an EMI 9235QA Photomultiplier tube (PMT), coupled to Schott BG-39 and Hoya U-340 optical filters. For Ed measurements, a standard 5-point single aliquot regeneration (SAR) protocol was adopted (Murray and Wintle, 2000). Preheating was done at 220 °C for 10 s; and a cut heat of 160 °C was used. The preheat temperatures were ascertained using dose recovery tests at a different temperature and recuperation ratio (see Supplementary data; Fig. 1sa and b). We found it difficult to remove the feldspar luminescence completely, hence, we performed an additional step of cleaning using infrared stimulation (145 mW/cm²; double SAR protocol; Jain and Singhvi, 2001). Typically, 30–35 discs were measured using photon counts initially of 0.8 s of the optical decay curve following subtraction of the background (8 s). Aliquots with a recycling ratio > 1 ± 0.1 were rejected and the mean of all palaeodoses was utilized for age computations.

Dose rate calculations used the elemental concentrations of U, Th and K, assuming radioactive equilibrium in the decay chains, which were measured using XRF and ICP-MS at the Wadia Institute of Himalayan Geology, Dehradun, India. Mean water content was assumed to be 5 ± 3% (for Indus sediments) and 10 ± 5% (Ganga and Brahmaputra

River sediments). The difference is because the Indus lies in the dry rain shadow zone of the ISM and the Brahmaputra and Alaknanda-Mandakini Rivers have wetter catchments. The cosmic dose rate was estimated as per Prescott and Stephan (1982). Paleodose estimation utilized the minimum age model (MAM, see Supplementary data)

The study utilized three AMS ages from the Kedarnath section (Mandakini River), four OSL ages at Jakhni (Alaknanda River), a combination of eight OSL and one AMS age at the Nimu section (Indus River), and four OSL ages from the Brahmaputra River valley. Table 1 provides details of the locations, dosimetry and age data of all the OSL samples. Table 2 details the AMS ages. AMS dating of charcoal samples was carried out at the Poznan Radiocarbon Laboratory, Poland; and the ages were calibrated using CalPal (www.calpal-online.de). Analyses for the OSL ages of the Jakhni section on the Alaknanda River were performed at the Physical Research Laboratory, Ahmedabad and the rest of the OSL dating was performed at the Wadia Institute of Himalayan Geology, Dehradun.

3.3. Paleoflood discharge estimate

Paleoflood discharge can be estimated via hydraulic modelling or by using empirical equations for bankfull discharge (Baker, 1987; Blum and Valastro, 1987). Bankfull discharge at a given cross section is the flow that fills the channel to the top of the bank, marking incipient flooding (Williams, 1978). Bankfull discharge is directly proportional to the channel width, hydraulic radius, and the channel slope (Dunne and Leopold, 1978). Determination of a paleoflood discharge from bankfull discharge and channel dimensions is problematic because (a) there is inherent variability in discharge for river channels with identical dimensions, despite the existence of power law relationships between river width, depth, and velocity (Leopold and Maddock, 1953), because of uncertainty in the data used for the equations; (b) lack of robust equations for all types of rivers; and (c) errors in estimating historic dimensions for a (potentially) unstable channel reach (Bauer and Klinger, 2010). Herein we attempt to account for this uncertainty by calculating several discharge estimates from a range of probable channel dimensions, and two different equations.

Williams (1978) developed a bankfull discharge equation for a dataset of 233 published and unpublished bankfull discharges:

$$Q = 4.0A^{1.21}S^{0.28} \quad (1)$$

where Q is discharge ($\text{m}^3 \text{s}^{-1}$), A is area (m^2), and S is dimensionless slope. Eq. (1) has a mean standard error of 41% and accounts for 96% of the sums of squares of log Q for the dataset from which it was determined (Williams, 1978). More recently, Bjerklie et al. (2005) suggested the following model for natural rivers:

$$Q = 7.14WY^{1.67}S^{0.33} \quad (2)$$

where Q and S are as above; W is channel width (m); and Y is mean channel depth (m). The coefficients were determined from over 1000 flow measurements from 103 rivers in the USA and New Zealand. In the determination, river slopes were obtained from reported values or extracted from topographic maps. Herein, we modify Eq. (2) by substituting Y with hydraulic radius (R); Y and R are assumed to be nearly equivalent when channel flows have a high width-to-depth ratio (Stokes et al., 2012), as is the case for our studied cross section:

$$Q = 7.14WR^{1.67}S^{0.33} \quad (3)$$

We attempt to minimize errors in the calculation of A by defining high-resolution trapeziums across the valley cross section. Valley width (W) was determined from the Shuttle Radar Topographical Mission (SRTM) Digital Elevation Model (DEM) of 90 m. Slope (0.004 ±

Table 1
Optically stimulated luminescence chronology of paleoflood sediments.

Field no.	Lab no.	U (ppm)	Th (ppm)	K %	Cosmic ray	Water content (%)	Mean ED (Gy)	Least ED (Gy)	Dose rate (Gy/ka)	Mean age (ka)	Least age (ka)
Alaknanda River											
JKN TL 1 (top)		5.6 ± 0.8	15.8 ± 2.7	2 ± 0.1	101 ± 10	10 ± 2		6.6 ± 0.9	4.6 ± 0.4		1.4 ± 0.2
JKN TL 2		4.5 ± 0.7	11.8 ± 2.4	2 ± 0.1	130 ± 13	10 ± 2		5.6 ± 0.7	4 ± 0.4		1.4 ± 0.2
JKN TL 3		4.4 ± 0.6	10.7 ± 2	1.8 ± 0.1	153 ± 15	10 ± 2		7 ± 1.1	3.7 ± 0.3		1.9 ± 0.3
JKN TL 4 (bottom)		4.7 ± 0.7	12.8 ± 2.4	2.4 ± 0.1	189 ± 19	10 ± 2		25 ± 1.8	4.6 ± 0.4		5.4 ± 0.5
Indus River											
IFP-1	LD-1651	2.2 ± 0.2	7.1 ± 0.7	1.52 ± 0.2	266 ± 81	5 ± 2	36 ± 8	30 ± 1	2.5 ± 0.0.2	13 ± 3	12 ± 1
IFP-3	LD-1652	1.8 ± 0.2	7.1 ± 0.7	1.38 ± 0.1	283 ± 85	5 ± 2	47 ± 10	32 ± 4	2.5 ± 0.1	19 ± 4	13 ± 2
IFP-5	LD-1653	1.9 ± 0.2	7.6 ± 0.7	1.39 ± 0.1	291 ± 87	5 ± 2	44 ± 7	34 ± 6	2.5 ± 0.1	17 ± 3	13 ± 2
IFP-8	LD-1654	1.7 ± 0.2	9.3 ± 0.9	1.6 ± 0.2	296 ± 90	5 ± 2	34 ± 8	29 ± 1	2.6 ± 0.2	12 ± 3	11 ± 1
IFP-12	LD-1655	1.9 ± 0.2	8.1 ± 0.8	1.58 ± 0.2	301 ± 90	5 ± 2	38 ± 6	31 ± 3	2.8 ± 0.1	14 ± 2	11 ± 1
IFP-14	LD-1656	2.6 ± 0.2	10.1 ± 1.0	1.91 ± 0.2	311 ± 93	5 ± 2	49 ± 9	36 ± 4	3.4 ± 0.2	14 ± 3	10 ± 1
IFPU-1	LD-1715	2.4 ± 0.2	11 ± 1.1	2.02 ± 0.2	347 ± 104	5 ± 2	44 ± 12	36 ± 1	3.2 ± 0.2	13 ± 4	11 ± 1
IFPU-2	LD-1716	1.9 ± 0.2	6.6 ± 0.1	1.73 ± 0.2	316 ± 95	5 ± 2	34 ± 6	26 ± 1	2.6 ± 0.2	13 ± 2	10 ± 1
Brahmaputra River											
Tuting TS-4	LD-520	2.3 ± 0.2	14.2 ± 1.4	2.5 ± 0.2	150 ± 30	10 ± 2		26 ± 1	3.5 ± 0.3		8 ± 1
Yinkiong											
YS-4	LD-551	1.8 ± 0.2	21 ± 2.1	2.7 ± 0.3	150 ± 30	10 ± 2		28 ± 4	4.3 ± 0.3		7 ± 1
Panging											
PS-1	LD-553	2.9 ± 0.3	16 ± 1.1	2.5 ± 0.3	150 ± 30	10 ± 2		29 ± 2	4.0 ± 0.3		7 ± 1
Geku											
SG-1	LD-677	1.9 ± 0.2	20 ± 2.0	2.5 ± 0.3	150 ± 30	10 ± 2		24 ± 2	4.0 ± 0.3		6 ± 1

0.0005) was determined from a 1:50:000 topographic map over a distance of 1000 m.

The flood deposits in the Alaknanda Valley at Jakhni at 12 ± 1 m a.r.l (R) where the channel has a width (W) of 245.5 ± 1 m. The cross section area (A) is 2738.5 ± 3 m² and the slope (S) is 0.003. With regard to the Indus River, the flood deposits of 2.04 m thickness are positioned 28.5 m above the present day river level. This elevation is approximately

20 ± 1 m above a valley fill terrace that is located at the confluence of the Indus and Zaskar Rivers (Blöthe et al., 2014; Dortch et al., 2011), approximately 1 km downstream from our study location. The terrace seats 10.5 m above the river. Thus, we assign R to be 20 ± 1 m. The width (W) is 270 ± 1 m; and the cross sectional area is 3927 ± 3 m².

The conservative error terms associated with W, S, R, and A above reflect our recognition of the uncertainties of estimating the channel dimensions associated with a historical time period. We also recognize the limitation that the equations used were not derived for the high mountain rivers we studied; but the basic equation used for such calculations remain same and we assume that the two equations bracket the plausible discharges.

3.4. Magnetic susceptibility and isothermal remnant magnetization (IRM)

Magnetic properties of a natural sediment sample depend upon many factors (Evans and Heller, 2003): (i) provenance (igneous, metamorphic and sedimentary); (ii) modifications of the mineral phase by physico-chemical reactions during transport; and (iii) diagenesis and bio-mineralization (Liu et al., 2012; Duan et al., 2014). We measured (i) magnetic susceptibility (χ_{lf}) that reflects the content of the magnetic fraction and (ii) Isothermal Remnant Magnetization (IRM) that depends upon the content of hematite or magnetite (Maher, 1988; Dearing,

Table 2
¹⁴C-AMS ages of flood sequence at Kedarnath and Indus valley.

Sample no.	Lab no.	Age ¹⁴ C (BP)	Calibrated age 2-sigma (BP)	Calibrated age 2-sigma (CE/BCE)
Kedarnath section, Mandakini River				
P6	Poz-65682	1175 ± 30	1108 ± 42	842 ± 45 CE
P7	Poz-65683	1140 ± 30	1048 ± 46	902 ± 46 CE
Po3	Poz-65680	1200 ± 30	1128 ± 42	822 ± 42 CE
Nimu, Indus River				
IFP	Poz-2-73572	12,014 ± 60	13,995 ± 208	12045 ± 208 BCE

1999; Thompson and Oldfield, 1986; Wang et al., 2004). Measurements were done using a Bartington MS2B sensor on ~10 g of sample packed in a nonmagnetic sample holder. IRM was acquired using an artificial forward magnetic field of 100 to 1500 mT with 100 mT increments. The magnetic moment was measured using a molspine spinner magnetometer and an artificial magnetic field was induced using an impulse magnetizer. These measurements were carried out only for the Indus River section because the geology of this section is composed of two mineralogically distinct lithologies – the sedimentaries of the Indus Molasse and Granitic rocks of the Ladakh Batholith. Provenance related studies of sequences for the Brahmaputra and Alaknanda Rivers were carried out by earlier workers (Lang et al., 2013; Wasson et al., 2013; Srivastava et al., 2008).

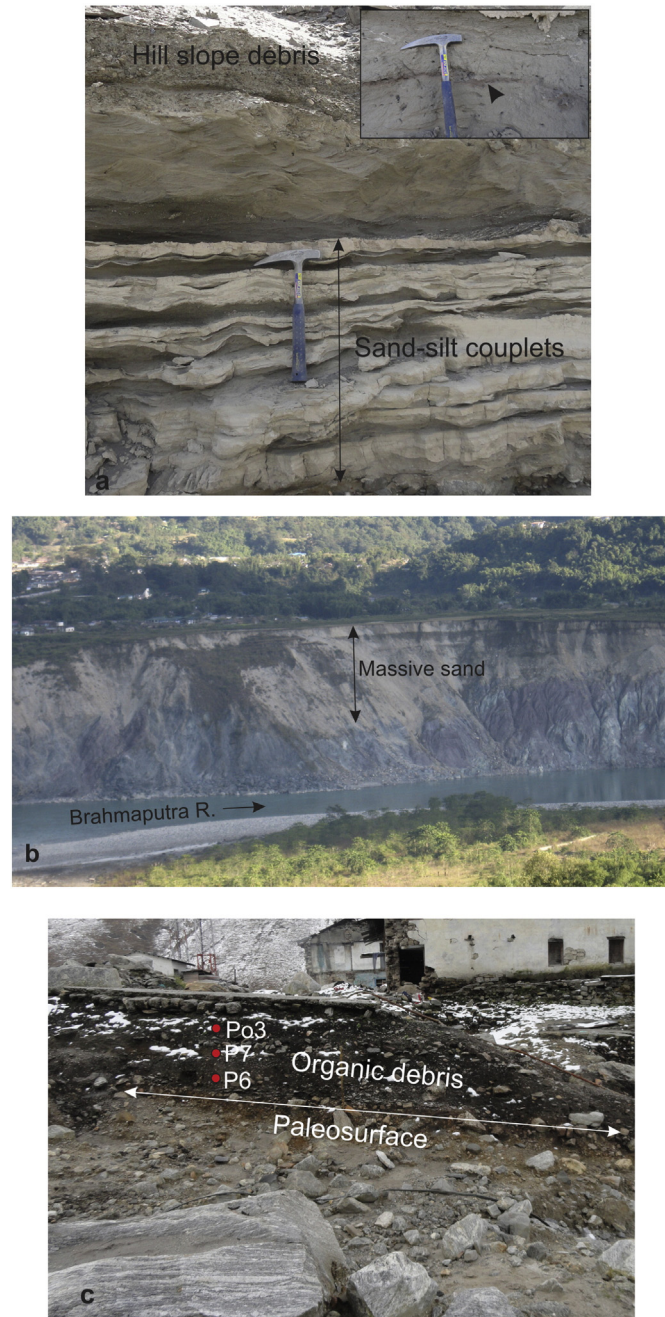


Fig. 4. Types of paleoflood deposits (a) Sand-silt couplets. Inset shows a layer with burnt charcoal (b) massive sand (c) organic debris flow. Refer to Fig. 5 for study sections and sample locations.

3.5. Pollen analysis

Three samples of flood deposits at Kedarnath were processed for pollen/spore analysis. Samples were prepared with the standard laboratory procedures of Moore et al. (1991) which included chemical treatment of samples with HCl, KOH and HF for removal of carbonates, silica minerals and humic substances. One *Lycopodium* spore tablet with ~10,680 spores was added to each sample for estimation of absolute frequency counts (Stockmarr, 1971, 1973). The slides were viewed under light microscope (Olympus BX 61) at 400× and 1000× magnifications for quantitative analysis minimum of 300 pollen grains were counted. The approximate number of pollen grains per gram in sediments was calculated using Maher (1981).

4. Results

4.1. Paleoflood evidence

Field observations indicate the presence of slack water deposits (SWDs), massive sand-silt beds, and organic-rich debris flow deposits at several sites. The slack water deposits are located at tributary junctions, in protected rocky shelters, or on river terraces. They typically appear as 5–30 cm thick flood couplets of grey to pale yellow fine sand and silt. Internally the sandy units are rippled with parallel lamination or are massive. Silty caps have fine lamination and are often moderately bioturbated. Where the flood deposits are adjacent to hillslopes, the succession is often punctuated by a unit of horizontally bedded hill slope debris. Every flood couplet has sharp basal and upper contacts. At the sites in the Indus and Alaknanda Rivers the tops of the units are marked by the presence of a burnt, red hearth layer containing angular pieces of charcoal (Fig. 4a). Similar paleoflood deposits from peninsular India have been described as SWDs (Baker, 1987; Ely et al., 1996; Kale et al., 1996, 2000). The couplets were deposited during the flooding into areas where flow velocities approach zero (Baker, 1987). Pedogenesis, bioturbation and burnt layers represent periods of landscape stability, while units of hillslope debris represent re-activation of hillslope during the flood occurrence.

Massive sand-silt beds are found on elevated bedrock benches and terraces. The beds typically consist of basal 0.5–5 m thick sandy units capped by 0.5–1.0 m thick bioturbated clayey silt. Internally, the sandy units are mostly massive with some ripples and parallel laminations, suggesting deposition by a rapid decrease in current velocity. The clayey silty caps are up to 10–50 cm thick and are bioturbated (Fig. 4b). These types of beds have been described as deposits of extreme floods resulting from the breaching of lakes formed by the damming of rivers/drainages (Montgomery et al., 2004). For example, the deposits of the 1970 extreme flood on the Alaknanda River, with similar sedimentary characteristics, occurred following the breaching of a landslide dam in the Birahi Ganga, a tributary of the Alaknanda River, along with LLOFs in other tributaries (Wasson et al., 2008). Lang et al. (2013) described similar deposits along the Brahmaputra River, and suggested that they are deposits of megafloods resulting from GLOFs in Tibet.

Organic-rich debris flow deposits occurring on the terraces are made up of black organic-rich clayey silt. Some contain pottery shards and sporadic angular gravels. Internally, the deposits are mostly massive but at places have weak bedding structures (Fig. 4c). Such deposits arise from extreme rainfall events that mobilize hillslope debris, erode agricultural fields, and inundate settlements. We found such deposits near Kedarnath, in the headwaters of the Mandakini River, a tributary of the Alaknanda River.

In the following sections we describe the stratigraphic sections and their chronology (Table 1). The samples showed no feldspar contamination in their shine-down or IRSL response curves, hence luminescence was detected using the SAR protocol (see Supplementary data for



Fig. 5. Paleoflood deposits in the headwaters of the Alaknanda-Mandakini river system, at Kedarnath. (a) General geomorphology of the area showing deposits of 2013 floods and outwash debris fan; Kedarnath Shrine (KS) and location of Paleoflood deposits (PFD); (b) flood deposits, note the presence of pottery shreds. Refer to Fig. 4c for complete profiles and sample locations; (c) types of pollen recovered from the profile. Refer to Fig. 1 for location.

details; Fig. 2s). All luminescence ages and one ^{14}C AMS age are in stratigraphic order, thereby providing confidence in the chronology

4.2. Alaknanda-Mandakini River

4.2.1. Kedarnath section

The stratigraphic section near Kedarnath (N30° 44'6.98" E79° 4'1.47") is located at the distal part of the debris fan of the Mandakini River, behind the Kedarnath Shrine, at an elevation of 3548 m amsl (above mean sea level). The area is in the headwaters of the river where, in 2013, excessive rain was added by the breaching of a moraine dammed lake, producing a massive flood in the river (Dobhal et al., 2013; Ziegler et al., 2014; Singh, 2014; Sundriyal et al., 2015). The 2013 event created an apron of fresh debris that flowed downstream then combined with other material in the village to form thick patches of mixed hillslope sediment, wood, and human wastes (Fig. 5a). As a result, the riverbed in the headwater reach of the Mandakini River aggraded by > 10 m (Sundriyal et al., 2015).

The section we examined contained a 1.9 m thick organic-rich debris flow deposits that formed at the distal part of a steep debris fan during past flood events (Figs. 4c and 5b). The sequence rests on an alluvial terrace surface and contains two units that mainly consist of organic-rich mud that fines upward with a basal coarse gravels (Fig. 4c). The mud dominantly contains silt with subordinate clay and sand. The gravels are 5–10 cm thick angular clasts of granodiorite and randomly scattered pottery pieces, which are flat, 2–10 cm wide, 1–2 cm thick, and are black and reddish in color. The foundations of the present Kedarnath Shrine have been constructed into this deposit.

Three samples of organic mud (samples P6, P7 and Po3) were analysed to document the vegetation that was contemporaneous with the deposits (see Fig. 4c for location). The key indicator taxon is the marshy Liliaceae that is found abundantly in all three samples, ranging in content from 16 to 19%. Additional pollen taxa are as follows: a) coniferous trees, *Abies pindrow* (1–3%) and *Pinus wallichiana* (1–2%); b) temperate, broad leaf taxa including *Quercus semecarpifolia* (9–15%), *Betula utilis* (3–6%) and *Alnus nepalensis* (4–6%); and c) herbaceous taxa (in samples P6 and Po3). Also in high frequency are the pollen of grasses (Poaceae), sedges, *Impatiens* (29 and 26%), Apiaceae (3 and 5%),

Artemisia (0.5 and 1%), Compositae (4 and 5%), Ranunculaceae (2%), and Caryophyllaceae (0.5%). Cerealia pollen grains also occur in high frequency in samples P6 and Po3 (29 and 27%) and occasionally in P7 as well along with abundant charcoal fragments that was the result of burning in the catchment, indicating that there was sufficient fuel, a condition that does not occur today (Fig. 5c). The pollen assemblage indicates that during the deposition of the debris flows the climate at Kedarnath was likely warm and wet, with marshy conditions where the temple now stands. The modern pollen spectrum of the region from the same location produced by Kar et al., 2016 suggests dominance of arboreals like *Pinus* (31–50%), *Alnus* (5–13%) followed by *Quercus* (1–9%) presently growing below ~3500 m altitude. Among non arboreals Lamiaceae, Polygonaceae, *Artemisia* and ferns is represented in good numbers. The dominance of Conifers over herbaceous taxa in the modern pollen spectrum is due to high pollen productivity and efficient wind dispersal to long distances which results their over representation in the pollen percent diagram. The modern pollen spectra suggests analogy of modern vegetation to the past with the occurrence of similar kind of vegetation.

Three samples of organic mud dated from different depths of the sequence yielded a mean (\pm Stdev) age of 1157 ± 22 BP (sample no P6, P7 and Po3). We infer these samples to be from a single event occurring during a warm phase in the 8th and 9th century CE (Table 2) that probably destroyed any existing settlement at Kedarnath. The present shrine was constructed following this event.

4.2.2. Jakhni section (30°13'39"N, 78°45'52"E)

A 4.6 m thick SWD containing eight flood units is located 12 m amsl on the right bank of Alaknanda River at Jakhni (520 m amsl; Fig. 6a,b). Each unit consists of a sand-silt flood couplet with a thickness of ~30–70 cm (Table 3; Fig. 6c). The basal parts of the couplets is made up of mica-rich coarse-to-fine sand capped by parallel laminations of clayey silt that are often broken laterally. The units also are occasionally capped by the accumulation of organic matter. OSL ages suggest that the oldest flood in the excavated part of the section (Unit 8) is about 5000 years old. Four floods (Unit 6 to Unit 2) occurred during the period 1.9–1.4 ka (Table 1; Fig. 6c). The top deposit has been identified as that of the 1970 flood by comparison with the sediments in the vicinity that are

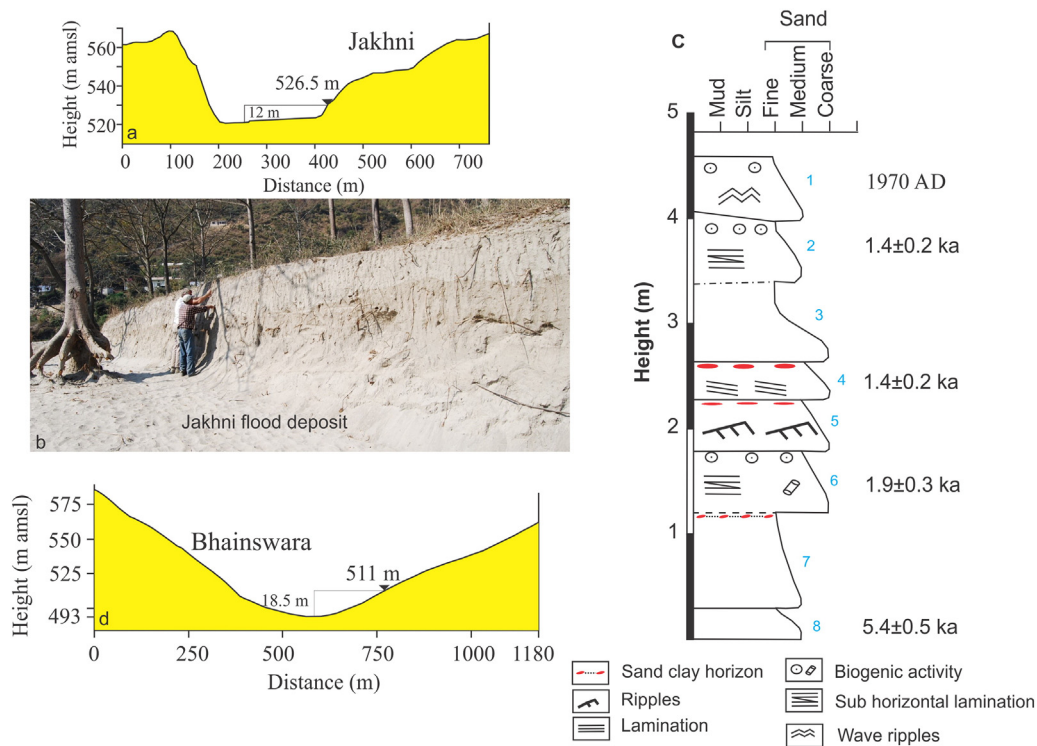


Fig. 6. Paleoflood deposits in the headwaters of the Alaknanda-Mandakini river system, located at Jakhni. (a) Channel cross section and location of paleoflood deposits at 3 m above the river level (arl); (b) photograph showing the flood deposits; (c) litholog and luminescence chronology of the paleoflood sequence; (d) cross section profile of the Alaknanda River at Bhainswara. Refer to Fig. 1 for locations.

known to have been deposited by that flood. The same flood unit was also found downstream at Bhainswara where its age was clearly known by local people (Wasson et al., 2013). We estimate the flood discharge ranged from $11,351 \text{ m}^3 \text{ s}^{-1}$ (Eq. (1)) to $16,347 \text{ m}^3 \text{ s}^{-1}$ (Eq. (3)), a range that spans the recorded peak discharge of the 2013 flood of $12,000 \text{ m}^3 \text{ s}^{-1}$ (S.P. Sati, pers. comm.).

4.2.3. Bhainswara, Deoprayag and Raiwala flood deposits

Wasson et al. (2013) studied the flood deposits at Bhainswara and Raiwala. Srivastava et al. (2008) examined similar deposits at Deoprayag (Fig. 1b). We revisited both sites. The Bhainswara section is located at an elevation of 511 m (amsl), 12 m above the river level of the Alaknanda River. This 6.5 m thick section has 11 SWD units with

ages in the range ~ 30 to 600 years BP (see Fig. 3 of Wasson et al., 2013). The Deoprayag section, consisting of two stacks of flood deposits, is located ~20 km downstream of Bhainswara. The younger stack, which is 4 m thick, lies at an elevation of 466 m amsl (9 m arl) and consists of at least five flood units that chronologically cluster at ~300 yrs BP. The older stack seats at an elevation of 473 m amsl (18 m arl) and is devoid of discernible flood units. It has an age of ~1.2 ka (Srivastava et al., 2008). Similarly, the Raiwala section located ~100 km downstream of Bhainswara, on the right bank of the Ganga River, consists of at least 14 flood couplets dating to between 1 and 0.7 ka (Wasson et al., 2013). At Bhainswara, the channel width (W) is $397 \pm 1 \text{ m}$, depth (R) is $18.5 \pm 1 \text{ m}$, slope (S) is 0.0042, and the channel cross section area (A) is $3672 \pm 3 \text{ m}^2$ (Fig. 6d). Discharge estimates at Bhainswara range

Table 3
Thickness, chronology and description of paleoflood deposits, Jakhni, Alaknanda valley.

Unit	Depth/thickness (cm)	Description	Chronology (ka)
Unit 1	0–61 (61)	Grey fine to medium mica-rich sand, well preserved wavy laminae, upper 13 cm pale brown fine sand (slight organic matter accumulation). Sharp inclined lower boundary	The 1970 deposit
Unit 2	61–122 (61)	Light grey brown fine to medium mica-rich sand, weak sub-horizontal plain laminae, upper 4–11 cm (with an irregular and gradational lower boundary) pale brown fine sand and shows accumulation of organic matter towards the top.	1.4 ± 0.2 (JKN TL 1)
Unit 3	122–195 (73)	Grey coarse to medium mica-rich sand, massive, pale brown compact fine to medium sand in the upper 20 cm and shows accumulation of organic matter towards the top	
Unit 4	195–230 (35)	Grey coarse to medium mica-rich sand, horizontal to inclined plain laminae, upper 2 cm brown (slight organic matter accumulation) massive coarse to medium sand with broken clay laminations	1.4 ± 0.2 (JKN TL 2)
Unit 5	230–280 (50)	Grey coarse to medium mica-rich sand, horizontal plain laminae and ripple laminae, upper 15 cm grey-brown compact massive medium to fine sand with clay laminae.	
Unit 6	280–340 (60)	Grey coarse to medium mica-rich sand, poorly developed sub-horizontal plain laminae, upper 15 cm brown-grey (slight organic matter accumulation in irregular patches suggesting bioturbation) fine to medium with a gradational lower boundary	JKN TL 3 1.9 ± 0.3
Unit 7	340–430 (90)	Light grey fine to medium mica-rich sand, massive, upper 3 cm compact sub-horizontal sandy clay laminae with sharp lower boundary	
Unit 8	430–460 (30)	Light brown fine to medium mica-rich sand, massive. Base not exposed	JKN TL 4 5.4 ± 0.5

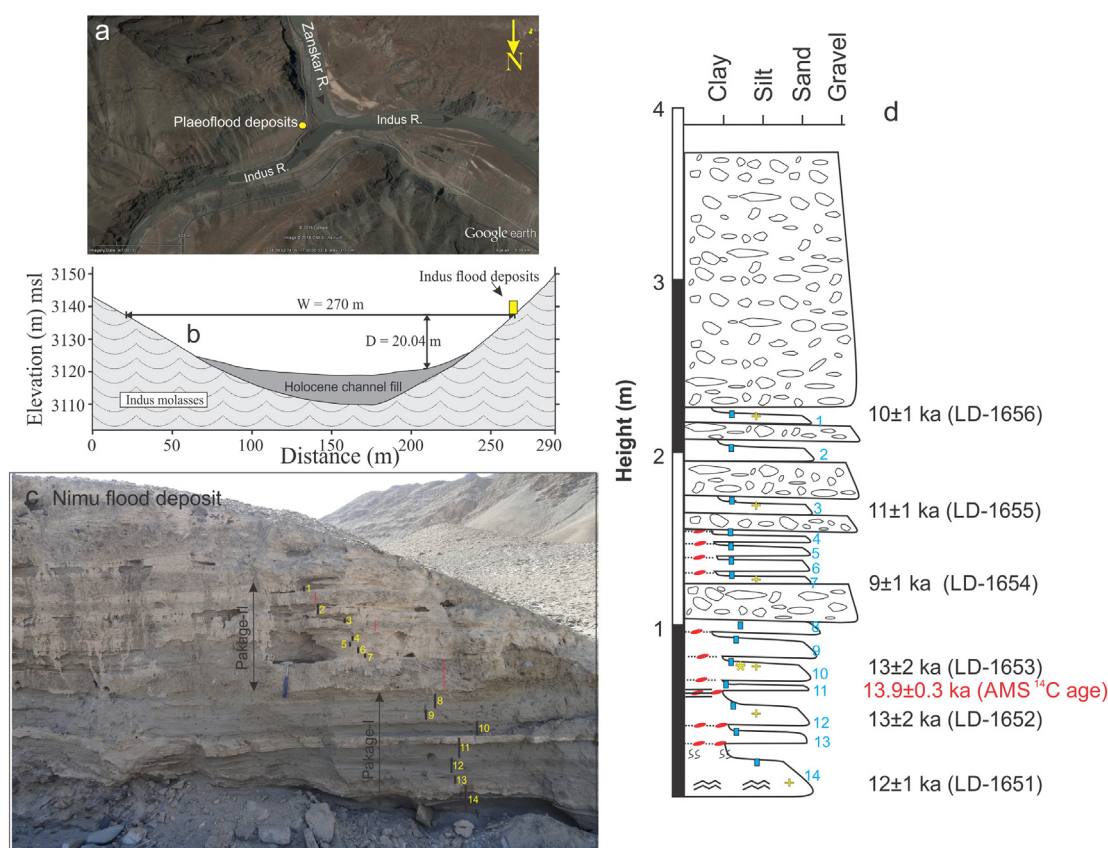


Fig. 7. (a) Google image showing location of paleoflood deposits at the confluence of the Indus-Zanskar rivers at Nimu, Ladakh; (b) channel cross section and hydraulic parameters of the Indus at the study site; (c) photograph showing the flood deposits and units; (d) litholog and luminescence chronology. Refer to Fig. 1 for locations.

from $25,175 \text{ m}^3 \text{ s}^{-1}$ (Eq. (1)) to $60,860 \text{ m}^3 \text{ s}^{-1}$ (Eq. (3)). Hydraulic modelling will be required to provide more accurate estimates.

4.3. The Indus River

At the Nimu section (N 34.16386° E 77.33234°) on the Indus River, a 2.04 m thick paleoflood record is present at the confluence of the Indus and the Zanskar Rivers (3154 m amsl; Fig. 7a), seating on a bedrock bench at 28.5 m (arl). The width of the active channel is 270 m (Fig. 7b). The deposits are typically 6–31 cm thick SWD couplets of basal fine sand capped by parallel laminated clayey silt (Table 4). The couplets are often separated by 10–20 cm thick beds of locally derived hillslope debris. Internally the hillslope units are weakly horizontally bedded, composed of 2–10 cm thick angular pebbles and gravels with approximately 10% of sand matrix. The sequence consists of 14 flood couplets, which, based on sedimentological characteristics, can be grouped into two packages (Fig. 7c). The basal package contains seven (Units 14 to 8) couplets of 6–31 cm thickness. Unit 10 (123–137 cm depth) contains a ~2 m wide and ~3 cm thick hearth with pieces of charcoal. The ¹⁴C AMS chronology of the charcoal from this unit yielded an age of 13.9 ± 0.2 ka cal BP (sample IFP, Table 2) with a luminescence age of 13 ± 1 ka from the same deposit (Table 1). The basal most unit (Unit-14) yielded a luminescence age of 12 ± 1 ka; and Unit 12 dated to 13 ± 2 ka. Thus, this package spans an age range of 14–12 ka.

The upper package also has seven 7–12 cm thick couplets (Units 7–1) that are frequently punctuated by hillslope deposits, consisting of 10–20 cm thick units of poorly sorted debris (Table 4). The package rests on a 20 cm thick layer of hillslope debris, overlain by four flood couplets of near uniform thickness (Units 4–7). Another three flood couplets are each separated by hillslope debris. Units 7, 3 and 1 are dated to 11 ± 1 ka, 11 ± 1 ka and 10 ± 1 ka, respectively (Fig. 7d). The upper package is has been traced laterally to ~50 m upstream into

the Zanskar River where the sequence seats on a bedrock bench and consists of at least seven discernible flood couplets. Luminescence dating of two units yielded similar ages (within the errors) of 11 ± 1 ka and 10 ± 1 ka (Table 1). Based on the existence of several units of hill-slope-derived sediment, we infer that the floods recorded in the upper package (Units 1–7) occurred during a time of high rainfall that activated hillslope erosion.

The magnetic susceptibility (χ_{lf}) and Isothermal Remnant Magnetization (IRM) data have a varying degree of linear association (Fig. 8). Flood couplets 3, 4, 5, 6, 7, 9, 12, 13 and 14 exhibit a strong linear relationship ($R^2 = 0.89$), suggesting that they have a single source. The magnetic mineralogy of this cluster shows a significant presence of ferrimagnetic minerals (magnetite) indicating that its source is an igneous body within the Ladakh Batholith, which occurs widely upstream in the Indus River valley (see Fig. 1c). Flood couplets 1, 8, 9 and 10 have a lower negative linear relationship between χ_{lf} and IRM ($R^2 = 0.61$), suggesting a mixing of sediments from granites of the Batholith and sedimentary material of the Indus Molasse (Fig. 1c). Couplet 2 also indicates a mixed source, but appears to be an outlier.

The cross section area (A), extending to the base of the flood deposit, and defined by a well resolved trapezium, is estimated to be $3927 \pm 3 \text{ m}^2$. Valley width (W) is an estimated 270 ± 1 m (Fig. 7b). The estimated discharges of the paleofloods ranges from $19,030 \text{ m}^3 \text{ s}^{-1}$ (Eq. (1)) to $47,954 \text{ m}^3 \text{ s}^{-1}$ (Eq. (3)).

4.4. Brahmaputra Valley

At Tuting (N28° 59' 50" E94° 53' 43.8"), situated at ~88 m arl, ~8 m of fine grained sand capped by a meter of thick clayey silt overlies an alluvial terrace (T-1) and is dated to 8 ± 1 ka (Fig. 9a). Earlier work on these deposits suggested that they are part of the terrace sequence (Srivastava and Misra, 2012), but their regional nature and petrography leads us to

Table 4
Thickness, chronology and description of paleoflood deposits, Nimu, Indus-Zanskar confluence, Ladakh.

Unit	Depth/thickness (cm)	Description	Chronology (ka)
Unit 1	0–7 (7)	5 cm thick dark grey coloured sand layer capped by a 2 cm thick parallel laminated clayey silt, moderately bioturbated and followed upward by a 1.5 m thick parallel bedded matrix supported hill slope debris.	LD-1656 10 ± 1
7–17 (10) hill slope debris			
Unit 2	17–29 (12)	10 cm dark grey fine sand capped by 2 cm thick parallel laminated clayey silt. Laterally, the silty layer is broken.	
29–49 (20) hill slope debris			
Unit 3	29–39 (10)	8 cm thick fine moderately bioturbated fine sand capped by 2 cm thick layer of parallel laminated clayey silt.	LD-1655 11 ± 1
39–49 (10) hill slope debris			
Unit 4	49–56 (7)	5 cm thick rippled fine sand capped by 2 cm thick massive clayey silt.	
Unit 5	56–64 (8)	6 cm thick dark grey coloured fine sand capped by 2 cm of clayey silt.	
Unit 6	64–73 (9)	7 cm thick rippled fine sand capped by 2 cm thick clayey silt	
Unit 7	73–81 (8)	5 cm thick bioturbated fine sand capped by 2 cm thick bed of clayey silt. The clayey bed is laterally discontinuous.	LD-1654 11 ± 1
81–101 (20) hill slope debris			
Unit 8	101–109 (8)	8 cm thick rippled fine sand	
Unit 9	109–123 (14)	10 cm thick rippled fine sand capped by 4 cm thick massive clay.	
Unit 10	123–137 (14)	12 cm thick grey fine sand capped by 2 cm thick clayey silt. The top of this layer shows a red color burnt layer with concentration of angular pieces of charcoal. The layer is ~3 cm thick and ~2 m wide.	LD-1653 13 ± 2 ¹⁴ C AMS 13,995 ± 208 yrs BP
Unit 11	137–143 (6)	5 cm fine sand capped by 1 cm thick clayey silt layer	
Unit 12	143–163 (20)	12 cm thick light grey, rippled fine sand capped by 8 cm thick parallel laminated clayey silt	LD-1652 13 ± 2
Unit 13	163–173 (10)	8 cm thick rippled fine sand capped by 2 cm thick clayey silt	
Unit 14	173–204 (31)	20 cm light grey rippled fine sand capped by 11 cm thick layer of bioturbated parallel laminated clayey silt	LD-1651 12 ± 1 ka

a new conclusion, namely they are deposits of megafloods. Further, ~75 km downstream at Yinkiong (N28° 39' 26" E95° 0'45.9"), a 6 m thick flood sequence made up of oxidized, parallel laminated fine sand, with bar and swell topography, is located at ~98 m arl on terrace

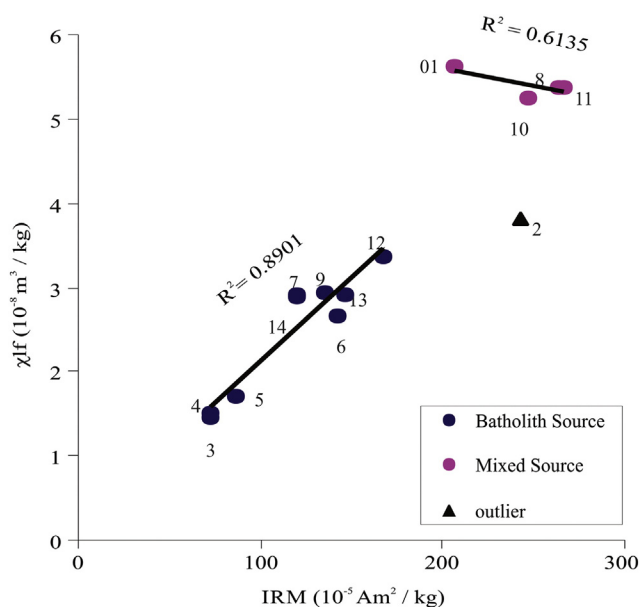


Fig. 8. Environmental magnetism data from the flood deposits of the Indus showing the two distinct sediment sources.

T-2 (Fig. 9b). The sequence is moderately bioturbated and is capped by a ~50 cm thick unit of clayey silt. A sample at a depth of 1.8 m has an OSL age of 7 ± 1 ka (Table 1). At Geku (N28° 25' 14.9" E95° 5' 23.7"), a similar 3.5 m thick sequence of parallel laminated, moderately bioturbated, oxidized fine sand is located on terrace T-1, and extends laterally for over 1 km on undulatory topography. The deposit seats at ~98 m arl. A sample from 1 m above the base is dated to 6 ± 1 ka (Table 1; Fig. 9c).

Similar fine grained sandy sequences dating to ~7 ka are found at Panging (N28° 13' 11.5" E94° 59' 48.1"; ~90 m arl) and at the mountain front near Pasighat (N28° 4' 25.9" E95° 23' 27.7") (Srivastava et al., 2009; Misra and Srivastava, 2009). The deposits indicate that the Brahmaputra valley experienced a megaflood between 6 and 8 ka BP. Further, Turzewski et al. (2014) reported deposits of two historical megafloods between 1200 and 1650 ¹⁴C yrs BP. They also found 18 SWDs between 27 and 10 ka BP on the Brahmaputra River. The Brahmaputra flood of 2000 CE is considered to have been the largest during the last century and the deposits of this flood are found on terraces and valley walls at elevations as high as 30 m arl (Evans and Delaney, 2011a,b). In contrast, the Holocene flood deposits sitting ~90 m arl seem to be higher than all other recorded floods and therefore are considered to be deposits of megafloods in the Brahmaputra (see Lang et al., 2013).

5. Discussion

5.1. Paleoclimate and floods in Mandakini-Alaknanda rivers

The debris flow sequence at Kedarnath (3548 m amsl), containing pottery shreds, is dated 1157 ± 22 cal yrs BP. The pollen record from

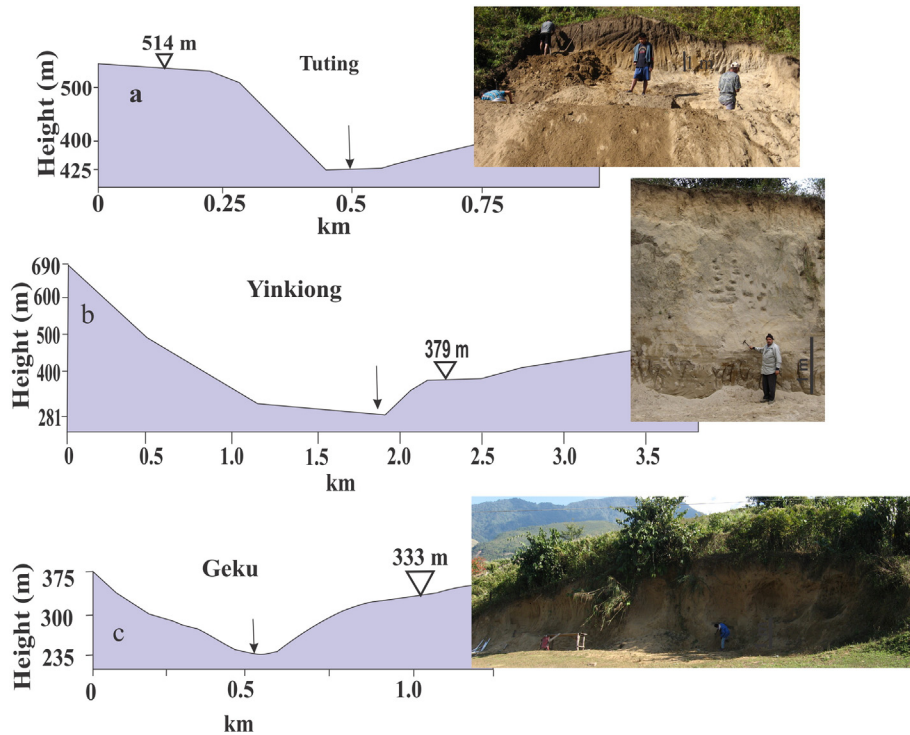


Fig. 9. Flood records from different locations in the Brahmaputra River valley, NE Himalaya. (a) Channel cross section, location and photograph of flood deposits at Tuting; (b) channel cross section, location and photograph of flood deposits at Yinkiong; (c) channel cross section, location and photograph of flood deposits at Geku. Refer to Fig. 1 for locations.

this flood deposit indicates an expansion of marshes during warm and humid conditions, a period associated globally with the Medieval Climate Anomaly (MCA). A peat record from Din Gad, a headwater tributary of the Ganga River, indicates the presence of warmth-loving broad leaf plants during the MCA (Fig. 10a; Phadtare, 2000). The pollen record from Chandra Tal (~4302 m a.s.l, N 33°79'40.5", E 78°34'27.4"),

Lahaul, Himachal Pradesh, NW Himalaya, also shows moderate warming around the MCA (Rawat et al., 2015a,b). The tree ring records from the western Himalaya further provide evidence of warming during this time (Singh et al., 2006).

At Jakhni (523 m amsl), a flood couplet that sits 3.5 m arl indicates an extreme event occurring about ~5 ka, when the pollen record in the peat sequence in the upper Ganga catchment showed increased presence of warmth-loving flora and tree taxa. The moderate flood at ~1.9 ka BP (unit 6) occurred when the climate record indicates a weaker monsoon (Phadtare, 2000; Fig. 10a). Further, four events clustered at ~1.4 ka (units 4, 3, 2) correspond with the MWP. The discharges during these floods are estimated to be between 11,351 m³ s⁻¹ (Eq. (1)) and 16,347 m³ s⁻¹ (Eq. (3)), although these values are highly uncertain. These MCA-related floods are also recorded further downstream at Deoprayag and Raiwala (Wasson et al., 2013).

In comparison, the Bhainswara flood sequence indicates a younger event dating between 600 and 30 a BP. The fact that the Bhainswara sequence is seating at 12 m arl and the valley is wider than at Jakhni indicates the recorded events are larger than those at Jakhni. The discharge during these floods is on the order of 25,175 m³ s⁻¹ (Eq. (1)) to 60,860 m³ s⁻¹ (Eq. (3)). Wasson et al. (2013) considered that most of the Bhainswara flood events resulted from LLOFs that were triggered by heavy rainfall events. Certainly, the events of 1894, 1970 and 2013 in the Garhwal Himalaya were partly related to LLOFs. Overall, the flood deposits in the Alaknanda-Mandakini valley indicate clustering of low-magnitude floods during the MCA and high magnitude floods involving LLOFs during the latter part of the millennium (600–30 a BP).

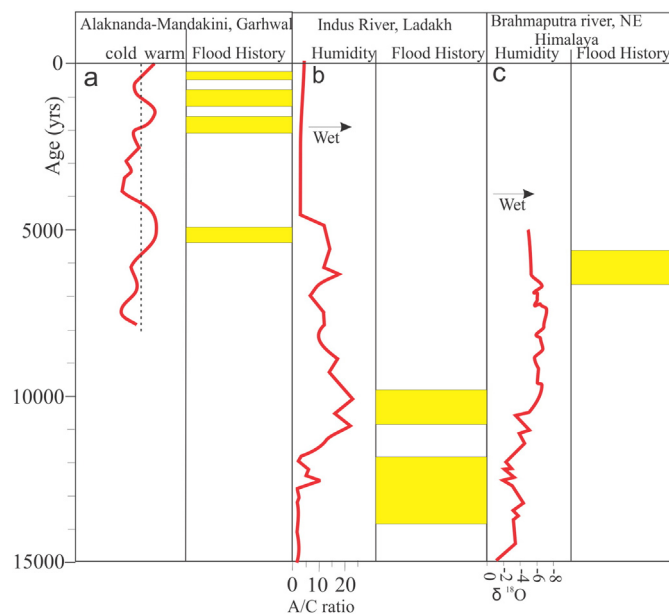


Fig. 10. Paleofloods in the Himalaya and past climate variability. (a) Climate data and paleofloods in the Indus River (climate data is taken from the Tso Kar lake record of Wünnemann et al., 2010); (b) climate data and paleofloods in the Alaknanda-Mandakini River (climate data has been extracted from the Din Gad Peat record at Gangotri, after Phadtare, 2000); (c) climate data and paleofloods in the Brahmaputra River (climate data are taken from a speleothem record from Meghalaya, NE India, after Dutt et al., 2015).

5.2. Paleoclimate and floods in the Indus River

The Indus River floods occurred in two phases, at 14–12 ka and 11–10 ka. Comparison of these floods with modern events is difficult because discharge data in the upper Indus Basin are not available, where there are few gauging stations, as data are not available in this strategically sensitive military area. Nonetheless, mean August discharge for the Indus River at Leh for the non-flooding years 2002, 2003 and 2004 is

$189 \pm 60 \text{ m}^3 \text{ s}^{-1}$. Further, $\sim 40 \text{ km}$ downstream at the Indus-Zaskar confluence at Nimu, a modelled estimate of mean August discharge is $\sim 850 \text{ m}^3 \text{ s}^{-1}$ (Mukhopadhyay and Dutta, 2010). The Indus River discharge measured by NHPC (National Hydro Power Corporation) at Alchi (14 km downstream from Nimu with no major tributary in between) during the 2006 and 2010 flash floods was $1846 \text{ m}^3 \text{ s}^{-1}$ and $1940 \text{ m}^3 \text{ s}^{-1}$, respectively (Thayyen et al., 2013). Discharge estimates from the early Holocene floods are much higher, ranging from $19,030 \text{ m}^3 \text{ s}^{-1}$ (Eq. (1)) to $47,954 \text{ m}^3 \text{ s}^{-1}$ (Eq. (3)). The large difference in discharge magnitudes between the early Holocene and modern floods points towards their different genesis.

Limited work on the 2010 flood suggests that it originated from an extraordinary climatic phenomenon that gained moisture and strength in the Leh Valley (Rasmussen and Houze, 2012; Kumar et al., 2014). This “cloud burst” driven event affected only three south flowing catchments near Leh, and therefore, the flooded area was limited, a conclusion reflected by a lower discharge in the Indus ($1940 \text{ m}^3 \text{ s}^{-1}$). The long-term trend of occurrence and forcing factors of such floods is largely unknown.

In Ladakh, the (reconstructed) climate records of the Holocene suggest that after the Last Glacial Maximum (LGM) humidity and precipitation increased from $\sim 14 \text{ ka BP}$, peaking at $12\text{--}10 \text{ ka BP}$. These variables then declined gradually until 7 ka BP . Both regained strength between 7 and 4.5 ka BP , and since 4.5 ka BP the climate has been largely drier, showing slight amelioration around the Medieval Climate Anomaly (Fig. 10; Demske et al., 2009; Wünnemann et al., 2010; Rawat et al., 2015a,b). These records indicate a strengthened ISM and widespread rainfall activity in Ladakh during the early Holocene. In the same period, the Indus and Zaskar Rivers experienced large floods.

The magnetic signatures of the flood sediments indicate a single provenance for most of the flood events in this period (flood couplet numbers 2, 3, 4, 5, 6, 7, 9, 12, 13 and 14). This finding, when viewed in conjunction with high discharges, indicates a flood mechanism involving LLOFs or GLOFs which can amplify flood discharges several fold.

The review by Hewitt and Liu (2010) indicates 71 GLOFs and LLOFs in the Karakoram since 1826, with events clustering around 1830, 1900, 1925 and 1970. We analysed these data in conjunction with reconstructions of temperature and rainfall from tree ring records in the rain shadow zone of the Himalaya over the past four centuries (Singh et al., 2006, Fig. 2b). The comparison indicates that clusters of GLOFs and LLOFs occur during times when rainfall was higher than normal and the temperature anomaly was between 0 and $-0.5 \text{ }^\circ\text{C}$. Therefore, the floods in the Indus River occurred during strengthened monsoon phases of the late Pleistocene-early Holocene, with flood magnitudes amplified by LLOFs and GLOFs.

5.3. Extreme floods in the Brahmaputra valley

In the upper Brahmaputra valley, cycles of glaciation and deglaciation during the Pleistocene led to the formation of several moraine dammed lakes with impounded volumes as high as $\sim 800 \text{ km}^3$ (Montgomery et al., 2004; Korup and Montgomery, 2008). The outbursts of these lakes generated megafloods with discharges exceeding $10^6 \text{ m}^3 \text{ s}^{-1}$ in the headwaters of the Brahmaputra valley (O'Connor et al., 2013). Available U-Pb data on the zircons of flood deposits indicate that they originated mostly in Tibet, and the floods evacuated huge volumes of sediment from the Tsangpo Gorge (Lang et al., 2013).

Our new data indicate that at least one of these floods occurred between 8 and 6 ka BP . Recent work indicates another such event occurred $1200\text{--}1650 \text{ yrs BP}$ (^{14}C); and 18 floods of varying sizes occurred between 27 and 18 ka BP (Turzewski et al., 2014). That study of paleoflood deposits in the Brahmaputra River reported 18 SWDs and evidence of two megafloods between 27 and 10 ka BP . Further, speleothem-based climate record from Mawmluh Cave, Meghalaya, NE India, indicates a relatively warm and wet phase between 8 and 6 ka BP and 23.3 and 17 ka BP (Dutt et al., 2015). The megafloods we dated and paleoflood

deposits dated by Turzewski et al. (2014) fall in these wet phases. Finally, reports of lake breaches in the headwaters of the Brahmaputra at $\sim 9 \text{ ka BP}$ (Montgomery et al., 2004), indicate that the megafloods in the Brahmaputra valley are consequences of a strengthened ISM.

6. Conclusions

Floods in the Himalaya result from the interaction between the Indian Summer Monsoon intensity and topography. On the southern front of the Himalaya, which receives $>2000 \text{ mm}$ of rainfall per annum, rivers flood almost every monsoon season. Sedimentary records of extreme floods are preserved in these rivers and the deposits of normal monsoon years are reworked and are therefore poorly preserved. In Ladakh, which lies in a high altitude desert within a rain shadow and receives $<100 \text{ mm}$ of annual rainfall, rivers flood only during abnormally wet monsoon years. Our new chronologically-constrained paleoflood deposits in the rivers of the Himalaya suggests the Alaknanda-Mandakini Rivers experienced floods during the Medieval Climate Anomaly. The deposits of these floods are preserved in the headwaters, mid reaches, and along the mountain front. The presence of pollen of warmth-loving species in debris flow deposits in the headwaters of the Mandakini River is additional evidence of wet conditions during that period. Large floods that involved LLOFs occurred during $600\text{--}30 \text{ yrs BP}$ in the Alaknanda River. Elsewhere, the Indus River, Ladakh, NW Himalaya, experienced extensive flooding during the Holocene climatic optimum. Data involving source parameters and paleodischarge estimates indicate that flood intensities were nearly an order of magnitude larger than modern floods. It is likely that GLOFs and LLOFs boosted flood magnitudes significantly. Finally, our results indicate the occurrence of a megaflood in Brahmaputra river valley, NE Himalaya, during $8\text{--}6 \text{ ka}$.

The major finding of this study is that on all timescales, from millennia to years, with one exception, extreme floods occurred when the ambient climate/weather were anomalously wet. The wet periods/years and therefore the extreme floods are caused by different climatic mechanisms, involving northward shifts in the influence of the monsoon, and local convective storms, often amplified by GLOFs and LLOFs. While the time lag between the generation of landslide lakes and LLOFs is not clear, it is possible that the climatic conditions that created the lakes were similar to those that created the floods by lake breaching. The mechanisms that created the glacial lakes by ice retreat or advance, and their relationships to wet periods and to GLOFs, has not been examined here and should be the subject of further research. Nevertheless, the coincidence of GLOFs with warm/wet periods suggests that high precipitation caused glacial lakes to fail, probably by overtopping. Also needed is an understanding of the geomorphic work accomplished by extreme floods in comparison with less extreme events. What is clear, however, is that the rivers of the Himalaya are susceptible to extreme floods on many timescales and future floods can be expected with or without significant human-induced climate change. The best currently available climate change projections suggest increasing temperature and heavy precipitation in the Himalaya in this century (Chaturvedi et al., 2012). These increases will likely produce floods, as our data indicate the area has a ‘natural’ proclivity for extreme floods to occur during warm and wet periods, a result of the ability of a warmer atmosphere to hold more precipitable moisture. The idea, promulgated by some commentators, that extreme floods, such as that of 2013 in the Mandakini River or of 2010 in Ladakh, are one-off events that are unlikely to reoccur is not supportable. Flood disaster risk reduction strategies are urgently needed, in the knowledge that extreme floods are common in the Himalaya, rather than relying solely on response in the aftermath of a deadly event. In the scenario global warming, what will be the contribution of glacial melt in causing floods is also a question to be explored in future.

Supplementary data to this article can be found online at <http://dx.doi.org/10.1016/j.geomorph.2016.12.011>.

Acknowledgements

Heads of WIHG, Department of Earth Science of IISc, Department of Geology of HNB Garhwal University, BSIP, PRL-India and NSU-Singapore are acknowledged for support. Studies in Kedarnath were conducted using grants from DST, New Delhi vide project number SB/S4/SE-682/2013. PS and RJ acknowledge funding from MoES (MoES/P.O.(Geosci.)/11/2013) vide project number MoES/P.O.(Geosci.)/11/2013. Work by the Singapore team was funded in part by two NUS-MOE grants (R-109-000134-112 and R-109-000-174-646). The project also benefited from the financial support of a Singapore Ministry of Education Academic Research Fund Tier 2 grant entitled 'Governing Compound Disasters in Urbanising Asia' (MOE2014-T2-1-017). Authors acknowledge the three anonymous reviewers for their comments that helped in improving the manuscript.

References

- Aitken, M.J., 1998. *An Introduction to Optical Dating*. Academic Press, London.
- Baker, V.R., 1987. Paleoflood hydrology and extraordinary flood events. *J. Hydrol.* 96, 79–99.
- Bauer, T., Klingler, R.E., 2010. Evaluation of paleoflood peak discharge estimates in hydrologic hazard studies. Report DSO-11-03. Dam Safety Technology Development Program. U.S. Department of the Interior Bureau of Reclamation Technical Service Center Geotechnical Services Division Seismotectonics and Geophysics Group Denver, Colorado.
- Bhutiyani, M.R., Kale, V.S., Pawar, N.J., 2010. Climate change and the precipitation variations in the northwestern Himalaya: 1866–2006. *Int. J. Climatol.* 30, 535–548.
- Bjerklie, D.M., Moller, D., Smith, L.C., Dingman, S.L., 2005. Estimating discharge in rivers using remotely sensed hydraulic information. *J. Hydrol.* 309, 191–209.
- Blöthe, J.H., Munack, H., Korup, O., Fülling, A., Garzanti, E., Resentini, A., Kubik, P.W., 2014. Late Quaternary valley infill and dissection in the Indus River, western Tibetan Plateau margin. *Quat. Sci. Rev.* 94, 102–119.
- Blum, M.D., Valastro Jr., S., 1987. Response of the Pedernales River of central Texas to late Holocene climate change. *Ann. Assoc. Am. Geogr.* 79, 435–456.
- Bookhagen, B., Thiede, R.C., Strecker, M.R., 2005. Late Quaternary intensified monsoon phases control landscape evolution in the northwest Himalaya. *Geology* 33, 149–152.
- Chaturvedi, R.K., Joshi, J., Jayaraman, M., Bala, G., Ravindranath, N.H., 2012. Multi-model climate change projections for India under representative concentration pathways. *Curr. Sci.* 103, 791–802.
- Dearling, J., 1999. *Environmental Magnetic Susceptibility Using the Bartington MS2 System*, second ed. Chinese Publications, Kenilworth.
- Demske, D., Tarasov, P.E., Wünnemann, B., Riedel, F., 2009. Late glacial and Holocene vegetation, Indian monsoon and westerly circulation in the Trans-Himalaya recorded in the lacustrine pollen sequence from Tso Kar, Ladakh, NW India. *Palaeogeogr. Palaeoclimatol. Palaeoecol.* 279, 172–185.
- Dobhal, D.P., Gupta, A.K., Mehta, M., Khandelwal, D.D., 2013. Kedarnath disaster: facts and plausible causes. *Curr. Sci.* 105, 171–174.
- Dortch, J., Owen, L.A., Haneberg, W.C., Caffee, M.W., Dietsch, C., Kamp, D.U., 2009. Nature and timing of large-landslides in the Himalaya and Transhimalaya of northern India. *Quat. Sci. Rev.* 28, 1037–1054.
- Dortch, J., Owen, L.A., Caffee, M.W., Kamp, U., 2011. Catastrophic partial drainage of Pangong Tso, northern India and Tibet. *Geomorphology* 125, 109–121.
- Doswell, C.A., 1985. *The operational meteorology of convective weather. Vol. II: Storm Scale Analysis*. NOAA Tech. Memo. ERL ESG-15, p. 240.
- Doswell, C.A., Brooks, H.E., Maddox, R.A., 1996. Flash flood forecasting: an ingredients-based methodology. *Weather Forecast.* 11, 560–581.
- Duan, Z., Liu, Q., Yang, X., Gao, X., Su, Y., 2014. Magnetism of the Huguangyan Maar Lake sediments, Southeast China and its paleoenvironmental implications. *Palaeogeogr. Palaeoclimatol. Palaeoecol.* 395, 158–167.
- Dunne, T., Leopold, L.B., 1978. *Water in Environmental Planning*. W.H. Freeman, San Francisco, CA (818 pp.).
- Dutt, S., Gupta, A.K., Clemens, S.C., Cheng, H., Singh, R.K., Kathayat, G., Edwards, R.L., 2015. Abrupt changes in Indian summer monsoon strength during 33,800 to 5500 years BP. *Geophys. Res. Lett.* 42, 5526–5532.
- Ely, L.L., Enzel, Y., Baker, V.R., Kale, V.S., Mishra, S., 1996. Changes in the magnitude and frequency of late Holocene monsoon floods on the Narmada River, central India. *Geol. Soc. Am. Bull.* 108, 1134–1148.
- Evans, S.G., Delaney, K.B., 2011a. Characterization of the 2000 Yigong Zangbo River (Tibet) landslide dam and impoundment by remote sensing. *Natural and Artificial Rockslide Dams*. Springer, Berlin Heidelberg, pp. 543–559.
- Evans, S., Delaney, K., 2011b. Characterization of the 2000 Yigong Zangbo River (Tibet) landslide dam and impoundment by remote sensing. In: Evans, S.G., et al. (Eds.), *Natural and Artificial Rockslide Dams*. Springer-Verlag, Berlin, pp. 543–559.
- Evans, M.E., Heller, F., 2003. *Environmental Magnetism: Principles and Applications of Environmental Magnetism*. Academic Press, p. 293 International Geophysical Series.
- Gadgil, S., 2003. The Indian monsoon and its variability. *Annu. Rev. Earth Planet. Sci.* 31 (1), 429–467.
- Gupta, V., Sah, M.P., 2008. Impact of the trans-Himalayan landslide lake outburst flood (LLOF) in the Satluj catchment, Himachal Pradesh, India. *Nat. Hazards* 45, 379–390.
- Hawks, J., Wang, E.T., Cochran, G.M., Harpending, H.C., Moyzis, R.K., 2007. Recent acceleration of human adaptive evolution. *Proc. Natl. Acad. Sci.* 104, 20753–20758.
- Hewitt, K., 1988. Catastrophic landslides and their effects on the Upper Indus streams, Karakoram Himalaya, northern Pakistan. *Geomorphology* 26, 47–80.
- Hewitt, K., 1998. Catastrophic landslide deposits in the Karakoram Himalaya. *Science* 242 (4875), 64–67.
- Hewitt, K., 1999. Quaternary moraines vs catastrophic rock avalanches in the Karakoram Himalaya, northern Pakistan. *Quat. Res.* 51, 220–237.
- Hewitt, K., Liu, J., 2010. Ice-dammed lakes and outburst floods, Karakoram Himalaya: historical perspectives on emerging threats. *Phys. Geogr.* 31, 528–551.
- Hobley, D.E., Sinclair, H.D., Mudd, S.M., 2012. Reconstruction of a major storm event from its geomorphic signature: the Ladakh floods, 6 August 2010. *Geology* 40, 483–486.
- Jain, M., Singhvi, A.K., 2001. Limits to depletion of blue-green light stimulated luminescence in feldspars: implications for quartz dating. *Radiat. Meas.* 33, 883–892.
- Johnson, C.N., Brook, B.W., 2011, December. Reconstructing the dynamics of ancient human populations from radiocarbon dates: 10 000 years of population growth in Australia. *Proc. R. Soc. B* 278 (1725), 3748–3754.
- Joseph, S., Sahai, A.K., Sharmila, S., Abhilash, S., Borah, N., Chattopadhyay, R., Pillai, P.A., Rajeevan, M., Kumar, A., 2014. North Indian heavy rainfall event during June 2013: diagnostics and extended range prediction. *Clim. Dyn.* 44, 2049–2065.
- Juyal, N., 2010. Cloud burst-triggered debris flows around Leh. *Curr. Sci.* 99, 1166–1167.
- Kale, V.S., 2004. Floods in India: their frequency and pattern. *Coping with Natural Hazards: Indian Context*. Orient Longman, Hyderabad, pp.91–103.
- Kale, V.S., Ely, L.L., Enzel, Y., Baker, V.R., 1996. Palaeo and historical flood hydrology, Indian Peninsula. *Geol. Soc. Lond., Spec. Publ.* 115, 155–163.
- Kale, V.S., Singhvi, A.K., Mishra, P.K., Banerjee, D., 2000. Sedimentary records and luminescence chronology of Late Holocene palaeofloods in the Luni River, Thar Desert, north-west India. *Catena* 40, 337–358.
- Kar, R., Bajpai, R., Mishra, K., 2016. Modern pollen rain in Kedarnath: implications for past vegetation and climate. *Curr. Sci.* 110, 296–298.
- Kochel, R.C., Baker, V.R., 1982. Paleoflood hydrology. *Science* 215, 353–361.
- Korup, O., Montgomery, D., 2008. Tibetan plateau river incision inhibited by glacial stabilization of the Tsangpo gorge. *Nature* 455, 786–789.
- Korup, O., Strom, A.L., Weidinger, J.T., 2006. Fluvial response to large rock-slope failures: examples from the Himalayas, the Tien Shan, and the Southern Alps in New Zealand. *Geomorphology* 78, 3–21.
- Kumar, A., Houze, R.A., Rasmussen, K.L., Peters-Lidard, C., 2014. Simulation of a flash flooding storm at the steep edge of the Himalayas. *J. Hydrometeorol.* 15, 212–228.
- Lang, K.A., Huntington, K.W., 2014. Antecedence of the Yarlung-Siang-Brahmaputra River, eastern Himalaya. *Earth Planet. Sci. Lett.* 397, 145–158.
- Lang, K.A., Huntington, K.W., Montgomery, D.R., 2013. Erosion of the Tsangpo Gorge by megafloods, eastern Himalaya. *Geology* 41 (9), 1003–1006.
- Leopold, L., Maddock Jr., T., 1953. The hydraulic geometry of stream channels and some physiographic implications. *U.S. Geol. Surv. Prof. Pap.* 252, 481–492.
- Liu, Q., Roberts, A.P., Larrasoana, J.C., Banerjee, S.K., Guyodo, Y., Tauze, L., Oldfield, F., 2012. Environmental magnetism: principles and applications. *Rev. Geophys.* 50, RG4002. <http://dx.doi.org/10.1029/2012RG000393>.
- Maddox, R.A., Hoxit, L.R., Chappell, C.F., Caracena, F., 1978. Comparison of meteorological aspects of the Big Thompson flood and Rapid City flash floods. *Mon. Weather Rev.* 106, 375–389.
- Maher Jr., L.J., 1981. Statistics for microfossil concentration measurements employing samples spiked with marker grains. *Rev. Palaeobot. Palynol.* 32 (2), 153–191.
- Maher, B.A., 1988. Magnetic properties of some synthetic sub-micron magnetites. *Geophys. J. Int.* 94, 83–96.
- Mason, K., 1929. Indus floods and Shyok glaciers. *Himal. J.* 1, 10–29.
- Misra, D.K., Srivastava, P., 2009. River response to continuing movements along the active faults in the Siang Valley, North-Eastern Himalaya, India. *Z. Geomorphol.* 53, 455–468.
- Montgomery, D.R., Hallet, B., Yüping, L., Finnegan, N., Anders, A., Gillespie, A., Greenberg, H.M., 2004. Evidence for Holocene megafloods down the Tsangpo River gorge, south-eastern Tibet. *Quat. Res.* 62, 201–207.
- Moore, P.D., Webb, J.A., Collinson, M.E., 1991. *Pollen Analysis*. Blackwell, Oxford, p. 216.
- Mukhopadhyay, B., Dutta, A., 2010. A stream water availability model of Upper Indus Basin based on a topologic model and global climatic datasets. *Water Resour. Manag.* 24, 4403–4443.
- Murray, A.S., Wintle, A.G., 2000. Luminescence dating of quartz using an improved single aliquot regenerative-dose protocol. *Radiat. Meas.* 32, 57–73.
- Negi, G.C., 2002. Hydrological research in the Indian Himalayan. *Curr. Sci.* 83, 974–980.
- O'Connor, J.E., Clague, J.J., Walder, J.S., Manville, V., Beebe, R.A., 2013. *Outburst floods. Treatise on Geomorphology*. Vol. 9, pp. 475–510.
- Phadtare, N.R., 2000. Sharp decrease in summer monsoon strength 4000–3500 cal yr B.P. in the Central Higher Himalaya of India based on pollen evidence from alpine peat. *Quat. Res.* 53, 122–129.
- Phartiyal, B., Sharma, A., Srivastava, P., Ray, Y., 2009. Chronology of relict lake deposits in the Spiti River, NW Trans Himalaya: implications to Late Pleistocene–Holocene climate-tectonic perturbations. *Geomorphology* 108, 264–272.
- Prescott, J.R., Stephan, L.G., 1982. Contribution of cosmic radiation to environmental dose. *PACT* 6, 17–25.
- Rana, N., Singh, S., Sundriyal, Y.P., Juyal, N., 2013. Recent and past floods in the Alaknanda valley: causes and consequences. *Curr. Sci.* 105, 1209–1212.
- Rasmussen, K.L., Houze Jr., R.A., 2012. A flash-flooding storm at the steep edge of high terrain: disaster in the Himalayas. *Bull. Am. Meteorol. Soc.* 93, 1713–1724.
- Rawat, S., Gupta, A.K., Sangode, S.J., Srivastava, P., Nainwal, H.C., 2015a. Late Pleistocene–Holocene vegetation and Indian summer monsoon record from the Lahaul, North-west Himalaya, India. *Quat. Sci. Rev.* 114, 167–181.

- Rawat, S., Gupta, A.K., Srivastava, P., Sangode, S.J., Nainwal, H.C., 2015b. A 13,000 year record of environmental magnetic variations in the lake and peat deposits from the Chandra valley, Lahaul: implications to Holocene monsoonal variability in the NW Himalaya. *Palaeogeogr. Palaeoclimatol. Palaeoecol.* 440, 116–127.
- Ray, Y., Srivastava, P., 2010. Widespread aggradation in the mountainous catchment of the Alaknanda–Ganga River System: timescales and implications to Hinterland–foreland relationships. *Quat. Sci. Rev.* 29, 2238–2260.
- Sati, S.P., Gahalaut, V.K., 2013. The fury of the floods in the north-west Himalayan region: the Kedarnath tragedy. *Geomat. Nat. Haz. Risk* 4, 193–201.
- Singh, D.S., 2014. Surface processes during flash floods in the glaciated terrain of Kedarnath, Garhwal Himalaya and their role in the modification of landforms. *Curr. Sci.* 106, 594–597.
- Singh, J., Park, W.K., Yadav, R.R., 2006. Tree-ring-based hydrological records for western Himalaya, India, since AD 1560. *Clim. Dyn.* 26, 295–303.
- Srivastava, P., Misra, D.K., 2012. Optically stimulated luminescence chronology of terrace sediments of Siang River, Higher NE Himalaya: comparison of Quartz and Feldspar chronometers. *J. Geol. Soc. India* 79, 252–258.
- Srivastava, P., Tripathi, J.K., Islam, R., Jaiswal, M.K., 2008. Fashion and phases of late Pleistocene aggradation and incision in the Alaknanda River Valley, western Himalaya, India. *Quat. Res.* 70, 68–80.
- Srivastava, P., Misra, D.K., Agarwal, K.K., Bhakuni, S.S., Luirei, K., 2009. Late Quaternary evolution of Ziro intermontane lake basin, NE Himalaya, India. *Himal. Geol.* 30, 175–185.
- Srivastava, P., Kumar, A., Mishra, A., Meena, N.K., Tripathi, J.K., Sundriyal, Y.P., Gupta, A.K., 2013. Early Holocene monsoonal fluctuations in the Garhwal higher Himalaya as inferred from multi-proxy data from the Malari paleolake. *Quat. Res.* 80, 447–458.
- Starkel, L., 1983. The reflection of hydrologic changes in the fluvial environment of the temperate zone during the last 15,000 years. In: Gregory, K.J. (Ed.), *Background to Palaeohydrology: A Perspective*. J. Wiley and Sons, pp. 213–235.
- Stockmarr, J., 1971. Tablets with spores used in absolute pollen analysis. *Pollen Spores* 8, 615–621.
- Stockmarr, J., 1973. Determination of Spore Concentration With an Electronic Particle Counter: Danmarks Geologiske Undersøgelse. *Årbog.* pp. 87–89.
- Stokes, M., Griffiths, J.S., Mather, A., 2012. Palaeoflood estimates of Pleistocene coarse grained river terrace landforms (Río Almanzora, SE Spain). *Geomorphology* 149, 11–26.
- Sundriyal, Y.P., Tripathi, J.K., Sati, S.P., Rawat, G.S., Srivastava, P., 2007. Landslide-dammed lakes in the Alaknanda Basin, Lesser Himalaya: causes and implications. *Curr. Sci.* 93, 568–574.
- Sundriyal, Y.P., Shukla, A.D., Rana, N., Jayangondaperumal, R., Srivastava, P., Chamyal, L.S., Juyal, N., 2015. Terrain response to the extreme rainfall event of June 2013: evidence from the Alaknanda and Mandakini River Valleys, Garhwal Himalaya, India. *Episodes* 38, 179–188.
- Teller, J.T., 1995. The impact of large ice sheets on continental palaeohydrology. In: Gregory, K.J., Starkel, L., Baker, V.R. (Eds.), *Global Continental Palaeohydrology*. J. Wiley and Sons, pp. 109–129.
- Thayyen, R.J., Dimri, A.P., Kumar, P., Agnihotri, G., 2013. Study of cloudburst and flash floods around Leh, India, during August 4–6, 2010. *Nat. Hazards* 65, 2175–2204.
- Thompson, R., Oldfield, F., 1986. *Environmental Magnetism*. Allen & Unwin, London, p. 227.
- Turzewski, M.D., Huntington, K.W., LeVeque, R.J., Feathers, J.K., Larsen, I.J., Montgomery, D.R., 2014. Megaflood erosion of the Tsangpo Gorge constrained by hydraulic modeling, geochronology, and geochemical fingerprinting. *AGU Fall Meeting Abstracts*. Vol. 1, p. 3506.
- Wang, H., Liu, H., Liu, Y., Cui, H., 2004. Mineral magnetism of lacustrine sediments and Holocene palaeoenvironmental changes in Dali Nor area, southeast Inner Mongolia Plateau, China. *Palaeogeogr. Palaeoclimatol. Palaeoecol.* 208, 175–193.
- Wasson, R.J., Juyal, N., Jaiswal, M., McCulloch, M., Sarin, M.M., Jain, V., Srivastava, P., Singhvi, A.K., 2008. The mountain-lowland debate: deforestation and sediment transport in the upper Ganga catchment. *J. Environ. Manag.* 88, 53–61.
- Wasson, R.J., Sundriyal, Y.P., Chaudhary, S., Jaiswal, M.K., Morthekai, P., Sati, S.P., Juyal, N., 2013. A 1000-year history of large floods in the Upper Ganga catchment, central Himalaya, India. *Quat. Sci. Rev.* 77, 156–166.
- Webster, P.J., Toma, V.E., Kim, H.M., 2011. Were the 2010 Pakistan floods predictable? *Geophys. Res. Lett.* 38 (4).
- Williams, G.P., 1978. Bank-full discharge of rivers. *Water Resour. Res.* 14, 1141–1154.
- Wünnemann, B., Demske, D., Tarasov, P., Kotlia, B.S., Reinhardt, C., Bloemendal, J., Diekmann, B., Hartmann, K., Krois, J., Riedel, F., Arya, N., 2010. Hydrological evolution during the last 15kyr in the Tso Kar lake basin (Ladakh, India), derived from geomorphological, sedimentological and palynological records. *Quat. Sci. Rev.* 29, 1138–1155.
- Ziegler, A.D., Wasson, R.J., Bhardwaj, A., Sundriyal, Y.P., Sati, S.P., Juyal, N., Nautiyal, V., Srivastava, P., Gillen, J., Saklani, U., 2014. Pilgrims, progress, and the political economy of disaster preparedness—the example of the 2013 Uttarakhand flood and Kedarnath disaster. *Hydrol. Process.* 28, 5985–5990.
- Ziegler, A.D., Cantarero, S.I., Wasson, R.J., Srivastava, P., Spalzin, S., Chow, W.T.L., Gillen, J., 2016. A clear and present danger: Ladakh's increasing vulnerability to flash floods and debris flows. *Hydrol. Process.* <http://dx.doi.org/10.1002/hyp.10919>.